Materials Today Advances 19 (2023) 100390

Contents lists available at ScienceDirect

Materials Today Advances

journal homepage: www.journals.elsevier.com/materials-today-advances/

Hf/porphyrin-based metal-organic framework PCN-224 for CO_2 cycloaddition with epoxides

Sergio Carrasco [a, b, *], Gisela Orcajo [a], Fernando Martínez [a], Inhar Imaz [c], Safiyye Kavak [d], Daniel Arenas-Esteban [d], Daniel Maspoch [c, e], Sara Bals [d], Guillermo Calleja [a], Patricia Horcajada [b, **]

[a] Chemical and Environmental Engineering Group, ESCET, Universidad Rey Juan Carlos, C/ Tulipán s/n, 28933, Móstoles, Madrid, Spain
[b] Advanced Porous Materials Unit (APMU), IMDEA Energy Institute, Avda. Ramón de la Sagra 3, E-28935, Móstoles, Madrid, Spain
[c] Catalan Institute of Nanoscience and Nanotechnology (ICN2), CSIC and The Barcelona Institute of Science and Technology, Campus UAB, Bellaterra, Barcelona, 08193, Spain
[d] EMAT and NANOlab Center of Excellence, University of Antwerp, Groenenborgerlaan 171, Antwerp, 2020, Belgium
[e] ICREA, Pg. Lluís Companys 23, 08010, Barcelona, Spain

ARTICLE INFO

Article history:
Received 17 April 2023
Received in revised form
6 June 2023
Accepted 7 June 2023
Available online 19 June 2023

Keywords:
MOF
Hafnium
Porphyrin
PCN
CO_2
Cycloaddition

ABSTRACT

Herein, we describe for the first time the synthesis of the highly porous Hf-tetracarboxylate porphyrin-based metal-organic framework (MOF) (Hf)PCN-224(M) (M = H_2, Co^{2+}). (Hf)PCN-224(H_2) was easily and efficiently prepared following a simple microwave-assisted procedure with good yields (56–67%; space-time yields: 1100–1270 kg $m^{-3}\cdot day^{-1}$), high crystallinity and phase purity by using trifluoromethanesulfonic acid and benzoic acid as modulators in less than 30 min. By simply introducing a preliminary step (10 min), 5,10,15,20-(tetra-4-carboxyphenyl)porphyrin linker (TCPP) was quantitatively metalated with Co^{2+} without additional purification and/or time consuming protection/deprotection steps to further obtain (Hf)PCN-224(Co). (Hf)PCN-224(Co) was then tested as catalyst in CO_2 cycloaddition reaction with different epoxides to yield cyclic carbonates, showing the best catalytic performance described to date compared to other PCNs, under mild conditions (1 bar CO_2, room temperature, 18–24 h). Twelve epoxides were tested, obtaining from moderate to excellent conversions (35–96%). Moreover, this reaction was gram scaled-up (x50) without significant loss of yield to cyclic carbonates. (Hf)PCN-224(Co) maintained its integrity and crystallinity even after 8 consecutive runs, and poisoning was efficiently reverted by a simple thermal treatment (175 °C, 6 h), fully recovering the initial catalytic activity.

1. Introduction

CO_2 emissions are one of the most concerning challenges that our society is facing nowadays [1–4]. Although the transition of the existing infrastructure from carbon-based sources to cleaner alternatives would be ideal, many of the proposed technologies are not yet sufficiently developed to facilitate large-scale implementation [5]. Besides more severe legislations, the discovery of new materials with suitable sorption/catalytic properties for application in real-world systems is an urgent need in the short to mid-term [6,7].

Metal-organic frameworks (MOFs) are crystalline porous coordination polymers consisting of polydentate organic linkers and metal cations, that have proven to be useful as catalysts due to the presence of accessible coordinatively unsaturated metal sites (CUS) [8,9]. In addition, their high regular micro- and meso-porosity enables the fast diffusion of different chemical species to these numerous catalytic active sites. However, some limitations remain as a challenge, mainly reproducibility and stability, in terms of synthesis and performance, respectively [10,11].

MOFs based on tetravalent cations and polycarboxylate porphyrin linkers have particularly attracted the attention of the scientific community as potential catalysts for CO_2 transformation because of the presence of two potential catalytic sites [12]: i) the

* Corresponding author.
** Corresponding author.
E-mail addresses: sergio.carrasco@imdea.org (S. Carrasco), patricia.horcajada@imdea.org (P. Horcajada).

https://doi.org/10.1016/j.mtadv.2023.100390

structural metal cluster based on M^{4+} cations showing an extraordinary oxophilicity [13,14]; and ii) an extra divalent cation that can be allocated in the void corresponding to the polypyrrole macrocyclic ring of the linker. The synergetic effect between the Brønsted and Lewis acid character of i) and ii), respectively, has resulted in outstanding conversions and selectivity towards cyclic carbonates in CO_2 cycloadditions under mild reaction conditions [14–16].

In 2012, Hong-Cai Zhou reported the synthesis of the Porous Coordination Network (Zr)PCN-222 (MOF-545) and, one year later, (Zr)PCN-224, both based on Zr^{4+} and tetrakis(4-carboxyphenyl) porphyrin TCPP [17,18]. These two MOFs differ in the coordination of the structural metal, 8- or 6- for (Zr)PCN-222 and (Zr)PCN-224, respectively, resulting in remarkably different structures and physicochemical properties. (Zr)PCN-222 shows a hexagonal morphology with the 3D Kagome-like topology, 1D channels with 2 pore sizes of 1.2 and 3.2 nm, and a BET surface area of *ca.* 2000 $m^2\ g^{-1}$. (Zr)PCN-224 presents a cubic structure with 3D nanochannels (1.9 nm), a larger BET surface area (*ca.* 2600 $m^2\ g^{-1}$), and a higher chemical stability of up to pH 11 *vs.* pH 7 found in (Zr)PCN-222.

These MOFs have been successfully proposed as catalysts in a wide variety of reactions, including CO_2 cycloaddition with epoxides to obtain cyclic carbonates [12], CO_2 photoreduction to yield fuels [19], photo-oxidative condensation for the preparation of imines [20], or photocatalytic hydrogen generation [21], among others [13,22]. Unfortunately, when catalytic mechanism involves the CO_2 fixation to the structural metal cluster, the integrity of PCNs is usually compromised [23,24]. Carrasco et al. prepared (Zr)PCN-222 for the CO_2 cycloaddition of epoxides and aziridines to obtain the corresponding cyclic carbonates and oxazolidinones [12]. They observed that the conversion was maintained during 4 consecutive runs, but crystallinity and particle size significantly decreased upon successive catalytic cycles. Thus, the preparation of more stable and active MOFs is in strong demand.

Intrigued by (Zr)PCN-222 limitations, we speculated that decreasing the cluster coordination could enhance the catalytic activity. PCN-224 structure showing hexa-coordinated clusters should be more active than PCN-222 showing octa-coordinated clusters, providing additional space for catalysis [18]. Besides, despite its lower cluster coordination, PCN-224 shows an improved stability over PCN-222 counterpart [17]. In addition, replacing Zr^{4+} by Hf^{4+} must enhance the acidity of the cluster and the affinity towards CO_2 because of the higher oxophilicity of the latter cation, improving the overall catalytic performance (bond dissociation energies of 801 kJ mol^{-1} for Hf–O and 790 kJ mol^{-1} for Zr–O) [14]. Thus, in that sense, (Hf)PCN-224 emerges as a potential catalyst with outstanding properties for this chemical reaction. To date, however, its synthesis has not been reported and only one example of (Hf)PCN-222 has been described, demonstrating the scarce attention paid to Hf in favor of Zr when considering this MOF family [25].

In this work, we report the synthesis of (Hf)PCN-224 overcoming some of the synthetic issues classically found in solvothermal methods by using microwave radiation (*i.e.* faster reactions, higher efficiency, phase selectivity, lower cost and easier morphological control) [12,26]. Special attention was paid to the nature and coordination effect of the modulator during the protocol optimization. The synthesis of (Hf)PCN-224(Co) upon linker metalation with Co^{2+} was also studied until high phase purity was observed. The novel Hf-porphyrin structure was resolved by synchrotron XRD and the chemical stability evaluated for both metalated and non-metalated MOFs in different aqueous (pH 1–14) and organic media by UV–Vis spectroscopy (linker releasing), gravimetry (weight loss) and PXRD (structural integrity). Thermal stability was monitored by TGA and variable-temperature XRD. BET surface area was determined by nitrogen sorption and isosteric heat of adsorption was estimated from the CO_2 isotherms at different temperatures. Particle size and morphology were observed by scanning electron microscopy (SEM) and the pore size and cluster location determined from MOF nanocrystals using high-angle annular dark-field scanning transmission electron microscopy (HAADF-STEM). Using (Hf)PCN-224(Co) as model catalyst, CO_2 cycloaddition conditions were optimized (mol% MOF and cocatalyst, time and gas pressure) using epichlorohydrin. Other PCN materials were also prepared here following other procedures already described in the literature: (Zr,Hf)PCN-222(H_2) and (Zr)PCN-224(H_2) [12,18]. Twelve different epoxides were then tested in such reaction to obtain the corresponding cyclic carbonates, which are relevant green solvents, monomers to obtain polycarbonates, drug precursors or even electrolytes in lithium batteries, among other applications [27,28]. Finally, MOF recyclability was evaluated upon different thermal regeneration treatments.

2. Methods

2.1. Synthesis of (Hf)PCN-224(H_2)

The procedure was adapted from the literature including some minor modifications [12]. Briefly, $HfOCl_2{\cdot}8H_2O$ (263.0 mg, 0.642 mmol) and benzoic acid (2.49 g, 20.43 mmol) were mixed in a 30-mL a microwave vial with 8 mL DMF. The cluster formation was performed at 140 °C for 5 min under stirring (600 rpm, 0 bar). After cooling, the previous cluster solution was poured in another vial containing TCPP (99.3 mg, 0.125 mmol) and 4 mL of DMF, and the new mixture was homogenized in an ultrasonic bath for 1 min. Trifluoromethanesulfonic acid (0.25 mL, 2.82 mmol) was rapidly added and the vial was immediately closed. The MOF synthesis was performed at 150 °C for 20 min under stirring (600 rpm, 3.9 bar). The minimum required power (within 0–15 W) was applied to maintain the temperature in both steps. Crystals were collected by centrifugation (10000 rpm, 10 min) and washed with absolute ethanol (3x30 mL, 10000 rpm, 10 min). The solid was finally resuspended in 5 mL ethanol and dried in a glass vial at 100 °C for 12 h, obtaining 184.2 mg of (Hf)PCN-224(H_2) ($C_{144}H_{78}N_{12}O_{64}Hf_{12}$, 67% yield based on metal basis).

2.2. Synthesis of (Hf)PCN-224(Co)

The procedure was similar to that described for the non-metalated counterpart but including a previous additional step and other minor modifications. TCPP (195.1 mg, 0.247 mmol) and anhydrous $CoCl_2$ (170.2 mg, 1.310 mmol) were mixed in a 30-mL microwave vial together with 6 mL DMF. Metalation was conducted at 175 °C for 10 min under stirring (600 rpm, 1.9 bar, 20 W). In parallel, the cluster solution was prepared using $HfOCl_2{\cdot}8H_2O$ (532.0 mg, 1.300 mmol) and benzoic acid (5.10 g, 41.76 mmol) with 6 mL DMF at 140 °C for 5 min (600 rpm, 0 bar). After cooling, cluster solution was poured on the metalation solution and then, trifluoromethanesulfonic acid was added (0.6 mL, 6.77 mmol) to finally conduct the polymerization at 150 °C for 30 min under stirring (600 rpm, 6.0 bar). Crystals were washed and activated following the above-mentioned procedure, obtaining 318.1 mg of (Hf)PCN-224(Co) ($C_{144}H_{72}N_{12}O_{64}Co_3Hf_{12}$, 56% yield based on metal basis).

2.3. Stability tests

10 mL of different solvents were added to 10 mg (Hf)PCN-224(H_2) in 30 mL glass vials under ultrasonic treatment (5 min, 40 °C) until homogeneous suspensions were obtained. Vials were placed in an orbital shaker (200 rpm, 24 h, room temperature) and materials were recovered by centrifugation and washed twice with absolute ethanol (13000 rpm, 8 min). After drying (100 °C, 24 h), weight losses were gravimetrically calculated in an analytical balance and crystallinity evaluated by PXRD. Different amounts of NH_4OH 28% wt., NaOH 2 M, HCl 37% wt. or PBS 0.5 M were used to control pH in aqueous media (1–13) and two different polymer concentrations were tested: 10 and 1 mg mL^{-1}. Polymers were subjected to an ultrasonic treatment under harsh conditions (1 h, 60 °C) and further washed and dried following a similar procedure as that described above.

2.4. Evaluation of linker releasing by UV–Vis spectroscopy

Initially, 10 mg of MOFs were suspended in 1 mL of each solution at the corresponding pH. Suspensions were treated in the ultrasonic bath for 1 h at 60 °C and centrifuged afterwards (13500 rpm, 5 min). 1 mL of DMF were added to each material, vortexed and sonicated for 1 min, and then centrifuged under similar conditions in order to wash TCPP remaining stack to the polymer. Both aqueous and organic fractions were mixed (2 mL in total) to be analyzed by UV–Vis spectroscopy. Only samples treated at pH = 12 were conveniently diluted (1/40) with H_2O:DMF 1:1, *v/v* prior to their measurement. MOFs were then washed twice with 2 mL ethanol and then dried at 100 °C for 12 h. The final weight of the material was used to determine the total amount of material lost during the overall process by gravimetry. This procedure was performed by triplicate for each polymer and pH value. UV–Vis measurements were performed inside quartz cuvettes within 800–300 nm wavelength range, after supernatant filtration with a 0.22 μm nylon filter. To evaluate the linker releasing, calibration using porphyrins was performed in a mixture of H_2O:DMF 1:1, *v/v* within 0.25–9.50 and 0.05–20.50 μM concentration ranges for TCPP(H_2) and TCPP(Co), respectively.

2.5. Catalytic tests

All the reactions were placed inside a stainless-steel reactor without stirring or additional solvents at room temperature. After purging the system with a continuous flow of CO_2 (2 min, 2 bar), the outlet valve was closed setting the desired pressure by controlling the inlet of the reactor. After catalysis, 2,3,5,6-tetrachloronitrobenzene (10–20 mol% respect to epoxide) was added as NMR internal standard to the reaction vessel. Extraction was performed with $CDCl_3$ (x3, 1.5 mL) and centrifuged in polypropylene tubes (13000 rpm, 5 min). The supernatant was filtered (nylon, 0.22 μm) prior NMR measurements. For a fixed amount of epichlorohydrin (0.02 mL, 0.255 mmol), different amounts of catalyst (Hf)PCN-224(Co) (0, 0.25, 0.5, 1 and 2 mol%, 0–9.1 mg) and co-catalyst TBAB (2.5, 5.0, 7.5 and 10 mol%, 1.0–4.0 mg) were tested for a fixed time (6 h) and temperature (24 °C) at two different CO_2 pressures (1 and 12 bar). Different reaction times were evaluated (1, 3, 6, 9, 15, 20 and 24 h) after finding the optimal conditions: epichlorohydrin (0.02 mL, 0.255 mmol), (Hf)PCN-224(Co) (1 mol%, 4.5 mg), TBAB (7.5 mol%, 2.95 mg) and CO_2 (1 bar). Different blank and reference tests (see Table S7) were performed under different conditions for a fixed amount of epichlorohydrin (0.02 mL, 0.255 mmol) and time (24 h).

Different PCN materials, *i.e.* (Zr)PCN-222(H_2), (Zr)PCN-224(H_2), (Hf)PCN-222(H_2) and their corresponding Co^{2+}-metalated counterparts, were prepared according to previously reported protocols in the case of PCN-222 series [12], or by simply replacing hafnium precursor by $ZrOCl_2 \cdot 8H_2O$ in the procedure described herein to obtain (Zr)PCN-224(H_2,Co). Similarly, $CoCl_2$ was substituted by the corresponding Ni^{2+}, Cu^{2+} and Zn^{2+} chlorides to yield (Hf)PCN-224(Ni, Cu or Zn). For comparison purposes, these materials were subjected to the same reaction conditions as described above for (Hf)PCN-224(Co): epichlorohydrin (0.02 mL, 0.255 mmol), PCN (1 mol%, different amounts according to their molecular weight), TBAB (7.5 mol%, 2.95 mg), CO_2 (1 bar) for 24 h. For scaling-up, similar reaction conditions were applied performing the reaction with the following amounts: epichlorohydrin (1.0 mL, 12.8 mmol), (Hf)PCN-224(Co) (1 mol%, 225.0 mg), TBAB (7.5 mol%, 154.4 mg), CO_2 (1 bar) for 24 h. The product was extracted with ethyl acetate (x2, 15 mL), the solvent evaporated under reduced pressure and finally purified by column chromatography (SiO_2; hexane/ethyl acetate 8:2). The substrate scope was evaluated for 12 epoxides: 1,2-epoxypropane (propylene oxide), 1,2-epoxybutane (butylene oxide), 1,2-epoxypentane (pentene oxide), 1,2-epoxyhexane (hexene oxide), 1,2-epoxytetradecane, 1-chloro-2,3-epoxypropane (epichlorohydrin), 2,3-epoxy-1-propanol (glycidol), 3,3-dimethyl-1,2-epoxybutane, 1,2-epoxy-2-methylpropane, 3,4-epoxy-1-butene (butadiene monoxide), 1-allyloxy-2,3-epoxypropane (allyl glycidyl ether) and 1,2-epoxyethylbenzene (styrene oxide) under previously optimized conditions: epoxide (different volumes, 0.255 mmol), (Hf)PCN-224(Co) (1 mol%, 4.5 mg), TBAB (7.5 mol%, 2.95 mg), CO_2 (1 bar) for 24 h. For recyclability tests, the material was washed with absolute ethanol (x2, 2 mL) after extraction with $CDCl_3$ and dried at 100 °C for 12 h. Similar amounts of epichlorohydrin and TBAB were added in each cycle until run 7. After this run, the regeneration of the catalyst was evaluated upon different thermal treatments: 150, 175 and 200 °C for 6 and 12 h, and then subjected to a new catalytic cycle under similar reaction conditions.

3. Results and discussion

In this work we firstly optimized the microwave-assisted synthesis of (Hf)PCN-224(H_2), focusing in the nature of the modulator. Afterwards, the preparation of (Hf)PCN-224(Co) was also optimized until phase purity was fulfilled.

3.1. Synthesis and characterization

3.1.1. Optimization of synthetic protocol

Note that several authors claim that the procedure to obtain Hf-based MOFs is as simple as replacing Zr by Hf precursors, ascribed to the same d^0 electronic configuration and having a similar radius because of the lanthanide contraction in the case of Hf^{4+} [29]. However, we observed that this statement could not be directly applied, probably due to the higher acidity of Hf^{4+} compared to Zr^{4+}, resulting in amorphous polymers, even further enhanced under microwave irradiation due to the excessive polarization of the electronic cloud [30]. Thus, synthetic conditions (nature and amount of modulators, temperature, and synthesis time) should be carefully optimized to produce a well crystallized and pure (Hf)PCN-224 material.

In a typical microwave procedure [12], the metal cluster is initially formed using the salt precursor in presence of benzoic acid (140 °C, 5 min). After the cluster stabilization, the MOF polymerization takes place under a second microwave irradiation step (150 °C, 20 min) by adding the TCPP linker and a modulator (see Supporting information; SI). Herein, we evaluated the effect of different acids as modulators (trifluoromethanesulfonic, methanesulfonic, trifluoroacetic, formic, acetic, propionic; Figure S2) and

their efficiency to replace the benzoate coordinated to the cluster to start nucleation and promote crystal growth. Trifluoromethanesulfonic acid (pKa = −14.7) was selected as the optimal candidate providing excellent crystallinity, morphology and yields (64 ± 4%, metal basis). Such a strong acid was required to break the Hf−O bond established with benzoate moieties and Hf^{4+}, without effectively coordinating the cation because of the steric hindrance of $-CF_3$ moiety and its poor donating ability, allowing the preferential interaction with the carboxylate units of the TCPP linker, more similar in form and acidity (pKa = 3.20−3.75) to the original benzoate molecules (pKa = 4.20) [31]. It should be noticed that using DMF as the synthesis solvent is essential both to solubilize the TCPP linker and to modulate the acidity-basicity of the overall system, thus controlling the deprotonation and coordination rate of TCPP to Hf^{4+}, regulated in return by the presence of the trifluoromethanesulfonic acid interacting with the solvent, as already proposed by Forgan in different systems [32]. This process occurred here in a fast and defective manner, critical for the stabilization of hexa-coordinated clusters, suggesting that the lower coordination mode of (Hf)PCN-224 can be achieved under kinetically controlled conditions favored by microwave heating [15]. This acid-base kinetically controlled equilibrium, responsible for the linker deprotonation and coordination, was essential as any other acid with higher pK_a (methanesulfonic, trifluoroacetic, formic, acetic, propionic) resulted in either amorphous solids or mixture of (Hf)PCN-222 and (Hf)PCN-224 phases (Figure S2) decreasing the polymerization rate and the amount of the material obtained, supporting our previous evidence.

After the optimization of (Hf)PCN-224(H_2), we further investigated the possibility to directly obtain the metalated MOF by simply introducing an additional microwave-assisted step, as reported elsewhere [12]. So, (Hf)PCN-224 was metaled with Co^{2+} since the mentioned work also demonstrated the outstanding performance of (Zr)PCN-222(Co) in CO_2 cycloaddition compared to other metalated homologues (Ni^{2+}, Cu^{2+} and Zn^{2+}), supporting the interest in this cation. Thus, the first step consisted of the Co^{2+} metalation of the TCPP(H_2) linker using a large stoichiometric excess (1:5) of $CoCl_2$ in presence of DMF (175 °C, 10 min), required to ensure a quantitative metalation of the linker. The role of the solvent in this process was critical to introduce divalent cations inside the porphyrin by deprotonating its N−H moieties. Surprisingly, unlike in the Zr-based analogues (*i.e.* (Zr)PCN-222(H_2)/(Zr)PCN-222(Co)), where both polymers were purely obtained independently on the use of TCPP(H_2) or TCPP(Co), here (Hf)PCN-224(Co) was obtained mixed with (Hf)PCN-222(Co) (*aprox*. 82 *vs.* 18% based on PXRD, Table S2, Figure S3) using the same composition than that resulting in pure (Hf)PCN-224(H_2). Using 4 equiv. in excess of Co^{2+}, while having a negligible impact on the (Zr)PCN-222 structure, revealed to be of great importance for the (Hf)PCN-224 formation. We speculated that, together with the higher Brønsted acid character of Hf^{4+}- compared to Zr^{4+}- cluster, Co^{2+} was also involved in the above-mentioned equilibrium participating as a Lewis acid coordinating triflate anions from the media and significantly modifying the apparent pH of the mixture [33]. To confirm this hypothesis, different amounts of trifluoromethanesulfonic acid were tested for a fixed pre-polymerization mixture (Table S2. 0.64 mmol Hf^{4+}, 20.3 mmol benzoic acid, 0.124 mmol TCPP, and 0.62 mmol Co^{2+} in 12 mL DMF). The amount of MOF significantly decreased by increasing the amount of the strong acid (from 160 to 55 mg using 1.1 or 5.5 mmol of acid, respectively). At lower acid concentrations than that of the standard mixture optimized for (Hf)PCN-224(H_2) (2.8 mmol), we observed an enrichment of (Hf)PCN-222(Co) phase by PXRD (Figure S3; see samples denoted A and B in Table S2 for compositions) indicating, as expected, a higher coordination of the cluster. As the acid concentration increased, the final polymer was richer in (Hf)PCN-224(Co) (Figure S4). The highest purity obtained in this test was 90% of (Hf)PCN-224(Co) (samples E and F with 4.0 & 4.5 mmol of trifluoromethanesulfonic acid, respectively). However, adding more than 5 mmol of the acid resulted in a higher (Hf)PCN-222(Co) content, being possible to obtain this phase pure with 5.5 mmol (sample denoted H; Table S2). Under such conditions, a higher rearrangement between linkers and clusters was observed because of the lower deprotonation rate, explaining the low yields (18%, related to (Hf)PCN-222 phase) observed and the higher coordination achieved.

So that favor higher nucleation rates and forcing a faster polymerization, while increasing the reaction yield, we decided to double the concentration of every reagent keeping intact the amount of solvent (12 mL DMF). For this experiment, we selected the sample D (3.4 mmol trifluoromethanesulfonic acid; Table S2, Figure S4) as a balance between purity (85% (Hf)PCN-224(Co)) and mass obtained. After this optimization, we were able to prepare pure (Hf)PCN-224(Co) in a good yield (55.4 ± 0.8%, metal basis) and crystallinity. This fast and efficient microwave method allowed to produce 1270 kg m^{-3} day^{-1} of (Hf)PCN-224(Co) and 1100 kg m^{-3} day^{-1} of (Hf)PCN-224(H_2). Space-time yields (STY) surpassed those reported for other MOFs being produced by industry during the early 2010s (*e.g.* (Al)MIL-53, (Cu)HKUST-1, (Fe)MIL-100 and (Zn) ZIF-8 with 160, 225, 20 and 100 kg m^{-3} day^{-1}, respectively) [34]. Note that current STY values achieved by microwave reactions could even reach 15000 kg m^{-3} day^{-1} (Al)MIL-53 [35], emphasizing the interest of microwave-assisted reaction from an industrial point of view.

PXRD patterns of (Hf)PCN-224(H_2) and (Hf)PCN-224(Co) were compared to that described for (Zr)PCN-224 (Figure S5), showing a perfect matching among them. Indeed, Le Bail analysis revealed a good fitting between the proposed structure and the experimental PXRD pattern (Figure S6). Note that because of the inherent capacity of microwave heating to yield small micro- and even nanometric crystals, the crystalline structure could not be resolved by conventional single crystal XRD methods, thus synchrotron radiation was used. Here, despite the low quality of the diffraction datasets, the obtained model confirmed that the structure of (Hf)PCN-224 is isoreticular to that previously described for (Zr)PCN-224 (see Supporting information; SI for further structural information: Table S3, Figure S7).

3.1.2. Physicochemical characterization

A full characterization (morphological, textural, compositional, etc.) of (Hf)PCN-224(H_2) and (Hf)PCN-224(Co) was carried out, paying special attention on their thermal and chemical stability.

Morphology and crystal size significantly differed between both the metalated and non-metalated MOFs. As observed by field emission scanning electron microscopy (FE-SEM), (Hf)PCN-224(H_2) crystals nucleated and grew as pseudo-spherical particles (540 ± 80 nm, n = 100 Fig. 1a and Figure S11a), whereas (Hf)PCN-224(Co) showed perfectly defined cubic crystals with truncated edges (3.0 ± 0.7 μm, n = 100 Fig. 1b and Figure S11b). In the first case, nucleation might be the most important process in detriment of growth, aspect typically observed for crystals resulting from kinetically controlled microwave reactions [36]. In contrast, thermodynamically stable phases are favored in solvothermal conditions, like in the case of (Zr)PCN-222, where growth was typically considered the controlling process of the crystallization, and thus providing larger well-faceted cubic microcrystals [12]. In order to support this hypothesis, we performed the solvothermal synthesis of (Hf)PCN-224(H_2) by using the similar pre-polymerization mixture than that used in the microwave protocol (120 °C for 16 h without stirring *vs.* 150 °C for 20 min under stirring), obtaining well-defined cubic crystals in the micrometric size range

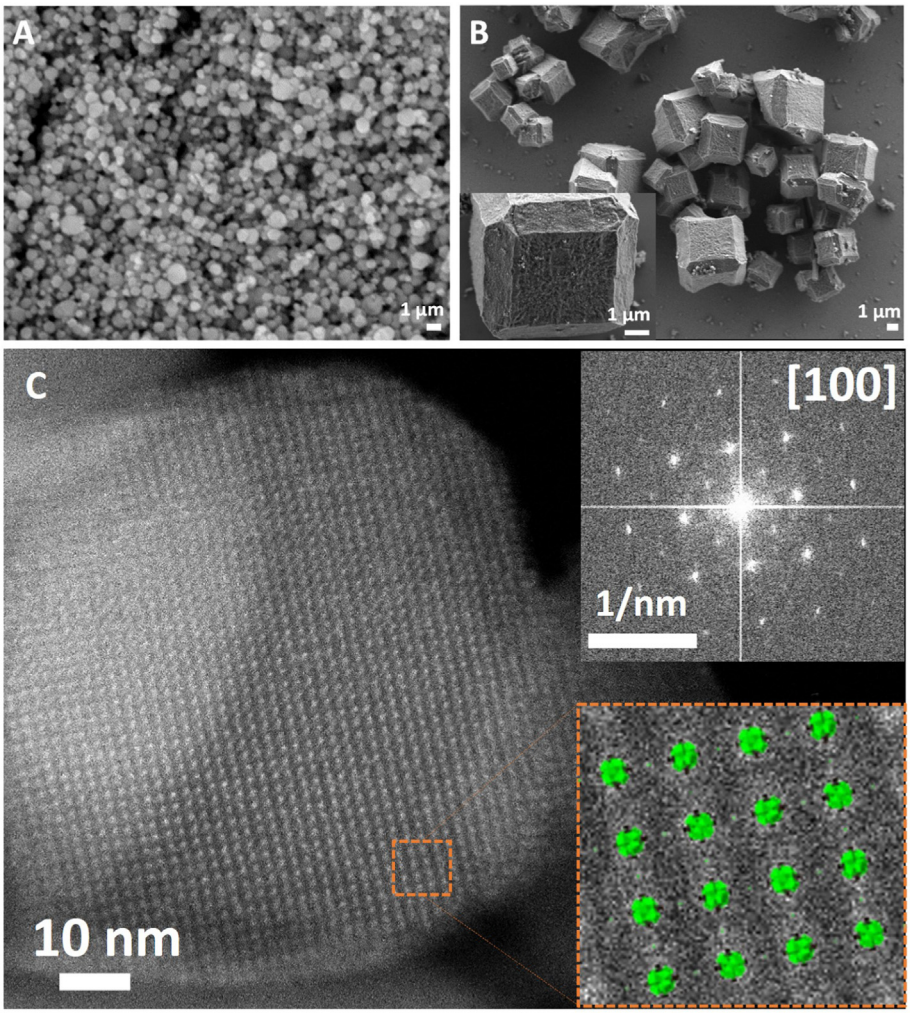

Fig. 1. FE-SEM images of: a) spheric-shaped (Hf)PCN-224(H_2) crystals at x10000; b) FE-SEM images of truncated (Hf)PCN-224(Co) crystals in [011], [101], [110] and their corresponding inverse directions at x3000 magnification (inset: x15000). c) High resolution HAADF-STEM image of a (Hf)PCN-224(Co) particle oriented along the [100] zone axis. Fast Fourier transform (FFT) of the image, confirming the crystal structure (top-right), and the theoretical model for PCN-224 structures superimposed on a magnified area indicated by orange dotted rectangle (bottom-right). (For interpretation of the references to colour in this figure legend, the reader is referred to the Web version of this article).

(2.5 ± 0.8 μm; Figure S12a), one order of magnitude larger than those particles obtained under microwave heating, confirming thus that the growth process is favored over nucleation under solvothermal conditions. HAADF-STEM image acquired at low electron dose (181.35 $e^- A^{-2}$) of a particle oriented along the [100] zone axis from the (Hf)PCN-224(Co) sample (Fig. 1c) shows a very ordered porous structure with an average pore size of 1.9 nm (Figure S13), as described in literature for PCN-224 structures [18], allowing the visual confirmation of the PCN-224 structure.

Further, the larger crystal size of the metalated (Hf)PCN-224(Co) in comparison with the non-metalated could be related with the presence of Co^{2+} during polymerization, which seems to favor growth instead nucleation, despite the microwave-assisted synthesis. In fact, this extent was confirmed replacing Co^{2+} by Cu^{2+} to yield (Hf)PCN-224(Cu), further used for catalytic comparison purposes, where micrometric cubes of similar size to those observed for (Hf)PCN-224(Co) were obtained (Figure S12b). This aspect affected not only the crystal dimensions but also their polydispersity, as different growth rates resulted in a wide variety of particle sizes in the case of metalated MOFs (Figure S11c).

Materials were also spectroscopically characterized by attenuated total reflection – Fourier transform infrared spectroscopy (ATR-FTIR, Figure S14), which band assignment can be found in Table S4. Upon the linker coordination, the broad band of O–H around 3000 cm^{-1} in free TCPP(H_2) dramatically decreased its intensity, indicating the coordination with the metal cluster in both MOFs. Besides this band attributed to oligomeric acid species [37], the single band of monomeric COOH units at 3640 cm^{-1} disappeared after polymerization. This evidence was additionally supported by the hypsochromic shift of C=O and C–O bands (1685 and 1278 cm^{-1} in TCPP(H_2) to *ca.* 1730 and 1305 cm^{-1} in MOFs, respectively) and a significant decrease in their intensities, revealing the vibrational constraint of carboxylate moieties interacting with the metal ion units [20]. Another evidence of this interaction relied on the presence of the Hf–O band located at 667 cm^{-1} for both MOFs, negligible in TCPP(H_2) [38]. In addition, the sharp band at 1002 cm^{-1} in (Hf)PCN-224(Co) indicated the interaction between Co^{2+} and the N of pyrrol moieties [12]. The spectrum of the metalated MOF lacked typical N–H bands that can be found in TCPP(H_2) and (Hf)PCN-224(H_2) at *ca.* 3320 (stretching), 960 (bending in plane) and 700-710 cm^{-1} (bending out of plane), supporting the full metalation of (Hf)PCN-224(Co).

The relevant textural properties of both MOFs were measured by sorption isotherms of N_2 and CO_2. First, N_2 sorption measurements

at 77 K provided type-I isotherms, typical of microporous materials (Figure S8), with pore volumes and sizes of 1.57 ± 0.09 and 1.58 ± 0.08 $cm^3\ g^{-1}$ (single point method), and 2.2 and 2.1 nm (DFT method) for the non-metalated and Co-metalated MOFs, respectively. On the other hand, the branch at $p/p_0 = 0.05–0.16$ was used for the calculation of the Brunauer-Emmett-Teller (BET) surface area, obtaining 2408 ± 13 and 2218 ± 5 $m^2\ g^{-1}$ (Figure S9). Differences between both values can be ascribed to the smaller particle size observed for (Hf)PCN-224(H_2) and (Hf)PCN-224(Co) (540 ± 80 nm *vs.* 3.0 ± 0.7 μm). Note that these values agree with those observed for the Zr^{4+} counterpart in previous publications [18,39,40].

The adsorption/desorption capacity of both materials towards CO_2 was also tested by measuring the corresponding isotherms at 273 and 293 K (Figure S10). (Hf)PCN-224(H_2) and (Hf)PCN-224(Co) were able to adsorb up to 2.43 and 2.24 mmol g^{-1} (at 273 K and 760 mmHg), and 1.57 and 1.41 mmol g^{-1} (at 293 K and 760 mmHg), respectively. These values compared well to other PCN materials such as their Zr counterparts: (Zr)PCN-222(H_2) and (Zr)PCN-222(Co) are able to adsorb 2.51 and 2.55 mmol g^{-1} (at 273 K and 760 mmHg), and 1.67 and 1.72 mmol g^{-1} (at 293 K and 760 mmHg) [12]. In the case of (Hf)PCN-224, the non-metalated MOF offered higher CO_2 adsorption capacity since its more available space expressed by larger surface-to-volume ratio. Note that this phenomenon cannot be explained in the basis of CUS availability (416 mmol g^{-1} coming from Hf^{4+} and 436 mmol g^{-1} from Hf^{4+} and Co^{2+} in the non-metalated and metalated counterparts, respectively). The smaller particle size of (Hf)PCN-224(H_2) (540 ± 80 nm) resulted in a higher exposure of CUS than in the case of (Hf)PCN-224(Co) (3.0 ± 0.7 μm) for the same amount of material. However, affinity for the gas was found to be slightly higher in the latter (23.3 ± 0.8 *vs.* 21.3 ± 0.6 kJ mol^{-1}; estimated by the isosteric heat of CO_2 adsorption from the isotherms at different temperatures using the Clausius-Clapeyron equation) [41], because of the presence of Co^{2+}. Independently on the metalation, these values were significantly higher than those reported for (Zr)PCN-222(H_2 and Co) of 17.4 and 17.6 kJ mol^{-1}, respectively, and within the range of the best performing and well-stablished materials for the selective adsorption and separation of CO_2, such as modified silica gel particles (MCM-41-100, 0.66 mmol g^{-1}, 19.8 kJ mol^{-1}), zeolites (Na-4A, 1.61 mmol g^{-1}, 25.2 kJ mol^{-1}) and other MOFs [42], revealing (Hf)PCN-222 (H_2,Co) as promising CO_2 adsorbents.

Thermogravimetric analysis provided relevant information on the composition and thermal stability of both materials in complement with other techniques (energy-dispersive X-ray spectroscopy X-EDS, thermal-dependent XRD). In general, decomposition of (Hf)PCN-224(H_2) occurred faster than for (Hf)PCN-224(Co), suggesting that the presence of cobalt within the linker enhanced its integrity (Figure S15) [12,20]. The main weight losses were observed at 395 and 470 °C, respectively, corresponding to the decomposition of the organic linker. In general, three significant weight variations can be observed in PCN materials. The first (up to 100 °C), similar in both MOFs (2 wt%), corresponded to small solvent molecules loaded within the porous structure, mainly ethanol used in the washing step. This was followed by the loss of −OH groups coordinated to metal clusters in a broad temperature range (150–300 °C) and cannot be separated from the last and most important weight loss, the abovementioned linker decomposition. Final residue was 48 and 52 wt% for (Hf)PCN-224(H_2) and (Hf)PCN-224(Co), respectively, in agreement with the theoretical amount of residual oxides after decomposition in air regarding their molecular formula: 49.1% (HfO_2) and 51.8% (HfO_2 + CoO). The experimental Hf/Co elemental ratio measured by X-EDS (12.6 ± 0.6) in (Hf)PCN-224(Co) matched well with the expected value (12.1), and the quantitative metalation was confirmed by inductively coupled plasma - optical emission spectroscopy (ICP-OES, Co^{2+} exp.: 3.3 ± 0.2%; theo.: 3.3%). Thermal stability was further investigated by variable temperature VT-PXRD (Figure S16). Last patterns showing measurable diffraction peaks were found at 340 and 400 °C for (Hf)PCN-224(H_2) and (Hf)PCN-224(Co), respectively. These values were 60–70 °C lower than those observed in TGA, suggesting a prior cluster discoordination before linker decomposition. After 570 °C, the unique presence of HfO_2 was observed (Figure S17).

The structural stability of (Hf)PCN-224(H_2, Co) was studied in the presence of different solvents (1 mg mL^{-1}, 24 h) by PXRD (Fig. 2). We observed an outstanding stability in all the tested organic solvents regardless their nature, including typical media for catalytic reactions, demonstrating the broad applicability scope of this material. Both polarity and solvent molecule size were somehow affecting the cluster coordination in different manners [43,44]. (Hf)PCN-224(H_2,Co) easily coordinate OH groups or water molecules taking the place of bidentate linkers without affecting the $Hf_6(O/OH)_8$ core [45]. For instance, considering protic polar solvents such alcohols, the trend of losing MOF weight was clearly defined: methanol>1-propanol>1-butanol (Figure S18), according to the length of the alkyl chain and supporting this evidence.

Finally, hydrolytic instability of many MOFs is a limiting factor for their application. Thus, the stability of (Hf)PCN-224(H_2) in aqueous media (10 mg mL^{-1}) at different pH values was explored (Figure S21). Weight losses were below 20% within the pH range 1–11, maintaining the structural integrity, which is in agreement with previous observations for (Zr)PCN-224 [18]. The MOF held its crystallinity even after using commercial HCl (37% wt.) but with higher weight losses (23%). At pH 13 or using NH_4OH (28% wt.), the structure was seriously damaged resulting in amorphous materials with weight losses higher than 60%. (Hf)PCN-224(H_2) was found to be stable in deionized water at 1 and 10 mg mL^{-1} concentrations (Figure S22). Crystallinity was unaltered using a phosphate buffer solution at low concentration (PBS 0.01 M, pH 7.4), but not using a higher salt content (PBS 0.5 M, pH 7.4) where 16% of the initial material was lost, becoming totally amorphous. On the other hand, tap water (sulfate content $<2\cdot10^{-4}$ M, total hardness $<5\cdot10^{-4}$ M in terms of $CaCO_3$, pH 6.8) was well-tolerated because of the lower salt content (12% weight loss and still crystalline). This lower stability in saline media has been reported before for other MOFs [46], but smartly exploited for purposes different from catalysis, such as drug delivery [23,47]. PXRD patterns at different pH values revealed the excellent structural stability of both MOFs even at low concentration (1 mg mL^{-1}, Figure S23), with a linker releasing below 2% within pH 7–11 monitored by UV–Vis spectroscopy (Table S6). Structural differences between (Hf)PCN-224(H_2) and (Hf)PCN-224(Co) were remarkably found at pH 1 and 12 based on a peak broadening effect (Figure S23a), suggesting a higher structural stability of (Hf)PCN-224(Co), similar to that observed at high temperature. Further details concerning the chemical and structural stability of these materials can be found in the Supporting Information.

3.2. Catalysis

Cycloaddition of CO_2 with epoxides was selected as our catalytic model reaction test because of the easy procedure, the clearance without the need of a solvent and the practical interest of cyclic carbonates [27]. In addition, when performed under mild conditions (room temperature), it results in negligible secondary sub-/by-products such as diols or polymers observed at higher temperatures [48–50]. In summary, it is considered one of the most efficient ways for CO_2 chemical fixation, being less energetically demanding than other conversion reactions such as

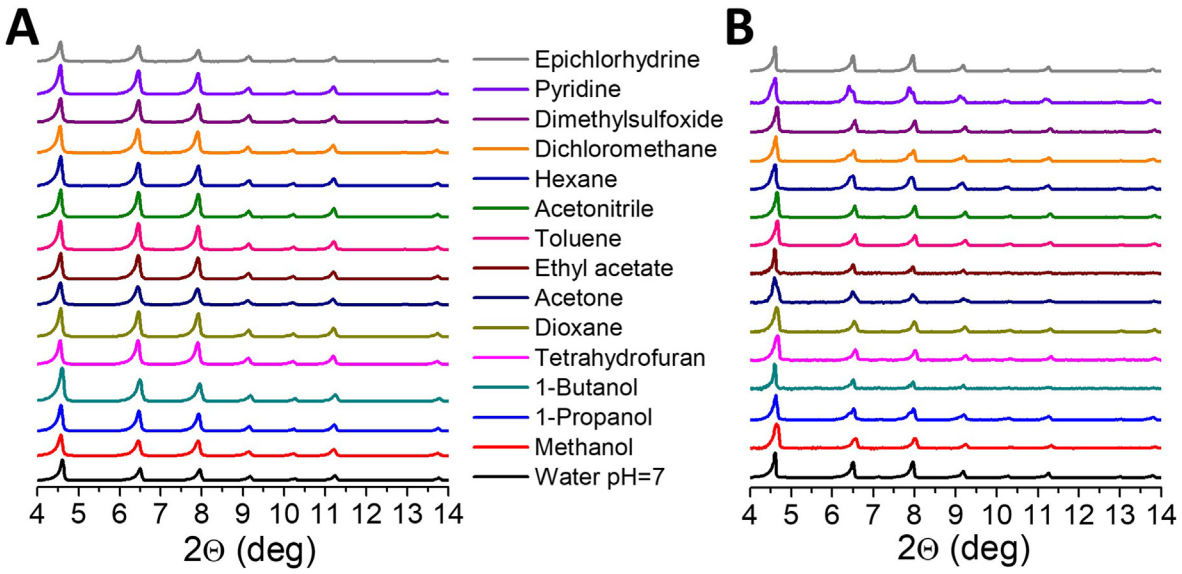

Fig. 2. PXRD patterns of: a) (Hf)PCN-224(H_2) and b) (Hf)PCN-224(Co) after treatment in different solvents (at room temperature, 24 h, 1 mg mL^{-1}, 200 rpm).

hydrogenations [10,13,27]. However, this reaction requires the presence of a co-catalyst responsible for the epoxide ring opening, typically halide anions in the form of tetrabutylammonium salts.

We proposed here (Hf)PCN-224(Co) as a promising candidate in CO_2 cycloadditions because of its higher chemical stability and availability of CUS compared to other well-known PCNs [12,18,51]. These previous works also demonstrated the superior catalytic activity of Co^{2+}-metalated PCNs compared to other metal ions and the non-metalated counterparts. The optimized conditions of the catalytic process can be found in SI.

Under optimized conditions (0.25 mmol epichlorohydrin, 1 mol % MOF, 7.5 mol% TBAB, 1 bar CO_2, 24 h, 24 °C; Figure S27), the catalytic performance of (Hf)PCN-224(Co) was compared to that of other non-metalated and Co^{2+}-metalated PCNs, as well as other (Hf)PCN-224(M) metalated counterparts, here prepared (M = Ni^{2+}, Cu^{2+}, Zn^{2+}; Table 1). No significant differences were found in terms of conversion between all the non-metalated MOFs (*i.e.* (Zr)PCN-222(H_2), (Zr)PCN-224(H_2), (Hf)PCN-222(H_2) and (Hf)PCN-224(H_2), 56–59%, entries 1, 3, 5 and 7), suggesting that both Zr^{4+} and Hf^{4+} structural ions contributed similarly to CO_2 cycloaddition under the optimized conditions for (Hf)PCN-224(Co), independently on their cluster coordination and Brønsted acid character. In contrast, it seems of great importance when MOFs were Co^{2+}-metalated. While (Zr)PCN-222(Co) and (Hf)PCN-222(Co) provided 74 and 73% conversion (entries 2 and 6), (Zr)PCN-224(Co) and (Hf)PCN-224(Co) resulted in 90 and 96% conversion (entries 4 and 8), respectively. First, it was evident that the CUS accessibility to hexa-coordinated clusters of PCN-224 is enhanced when compared to the octa-coordinated clusters found in PNC-222 [18]. Further, the higher oxophilicity of Hf^{4+} significantly increased the conversion compared to Zr^{4+} in the case of PCN-224 [14]. Intriguingly, the difference between both ions in terms of acidity was not evident in the case of the PCN-222 structure when is metalated with Co. This fact indicates a cooperative catalytic effect between the Lewis acid character of Co^{2+} and the Brønsted acid character of Zr^{4+}/Hf^{4+} cluster exclusively on PCN-224. Indeed, these results could be expected considering that the optimization was performed using (Hf)PCN-224(Co). Different structures (not only in terms of cluster coordination but also pore size, accessibility, and polar nature of cavities) and, more importantly, additional CUS modified the overall time to ensure the complete diffusion of reagents to catalytic sites and every step involved in the catalytic cycle: epoxide coordination, ring-opening, CO_2 addition and cyclic carbonate release. Kinetic equilibrium was achieved for (Hf)PCN-224(Co) after 24 h (Figure S28b).

Table 1
Conversions for different PCN materials in CO_2 cycloaddition of epichlorohydrin tested in this work.[a]

Entry	MOF	Metal	Conversion (%)
1	(Zr)PCN-222	(H_2)	59
2		(Co)	74
3	(Zr)PCN-224	(H_2)	57
4		(Co)	90
5	(Hf)PCN-222	(H_2)	57
6		(Co)	73
7	(Hf)PCN-224	(H_2)	56
8		(Co)	96
9		(Ni)	53
10		(Cu)	55
11		(Zn)	61

[a] Reaction conditions: 0.25 mmol epichlorohydrin, 1 mol% MOF, 7.5 mol% TBAB, 1 bar CO_2, 24 h, 24 °C.

Comparatively, to obtain similar epichlorohydrin conversions using (Zr)PCN-222(Co) as that found here for (Hf)PCN-224(Co) (95%: 1 mol% MOF, 7.5 mol% TBAB, after 20 h), it was required to harden the reaction conditions (89%: 2 mol% MOF, 10 mol% TBAB, after 18 h) [12]. Other authors have described a similar behavior on this basis for hexa- and octa-coordinated clusters in PCNs [15], and dodeca-coordinated cluster in UiOs [14], for the CO_2 photoreduction and glycerol acetalization, respectively. In the former work, Jin concluded that 6-linker connected systems based on M^{4+} should be regarded as missing linker defective systems, compared to ideal 12 linkers connected to $M^{4+}{}_6$-nodes. This was in agreement with the larger BET surface area and lower diffusion energy barriers found for PCN-224 compared to PCN-222, showing 3D and 1D channels, respectively [18,52]. In the case of non-metalated counterparts, the cooperative effect between both cations did not exist.

On the other hand, it is not a coincidence that most works have paid more attention to cobalt instead other divalent cations regarding metal-based Lewis acid catalysis using metalated porphyrins in Zr-based PCNs [12,18,51,53]. The higher efficiency of Co^{2+} has been explained as a multifactorial effect, but all of them

agree on the compromise between a moderate Lewis acid character and the convenient cation size, able of shifting out from the porphyrin plane [54–56]. The out-of-plane distortion together with the lower steric hindrance of reagents arranged around Co^{2+} compared to bigger cations are behind this relevant catalytic effect. To probe this explanation, the epichlorohydrin conversion was studied using (Hf)PCN-224(M) (M = Ni^{2+}, Cu^{2+}, Zn^{2+}) under optimized conditions for (Hf)PCN-224(Co). Interestingly, conversions (53–61%, Table 1, entries 9–11) were like that obtained using (Hf)PCN-224(H_2) as catalyst (56%), suggesting a negligible effect from the divalent cation located in the center of the porphyrin ring. This aspect was also observed before for (Zr)PCN-222(M), where (Zr)PCN-222(Ni and Cu) gave even lower yields (38 and 42%, respectively) than the non-metalated MOF (58%) in the CO_2 cycloaddition with 1,2-epoxynonane [12]. A similar trend was noted here (Co^{2+}>Zn^{2+}>H_2>Cu^{2+}>Ni^{2+}), independently on the MOF structure. Other works describing organometallic complexes based on planar ligands coordinated to divalent cations, *i.e.* M(salphen) catalysts (M = Ni^{2+}, Cu^{2+}, Zn^{2+}), for CO_2 cycloadditions with epoxides have reported similar results [57]. Nevertheless, the inverse catalytic activity was observed in Diels-Alder reactions, where the ability of Cu^{2+} and Ni^{2+} to form square planar complexes were critical to observe higher conversions, while Co^{2+} was the least efficient cation. Thus, we suspected that the preferential spatial disposition of the former cations inside the porphyrin, located in the same plane as N atoms of the pyrrole rings, could be behind the low activity of (Hf)PCN-224(Ni^{2+}, Cu^{2+} and Zn^{2+}) in CO_2 cycloadditions compared to (Hf)PCN-224(Co) since negligible out-of-plane distortions.

The reaction was successfully 50-times scaled-up (from 0.26 to 12.80 mmol) under similar reaction conditions. After purification by column chromatography, yield (1.45 g, 83%, isolated yield) did not significantly differ from the low scale reaction (86%, ^{1}H-NMR yield using internal standard). Turnover number (TON) and turnover frequency (TOF) of epichlorohydrin converted into the corresponding cyclic carbonate were 83 and 4 h^{-1}, respectively. The scope of the reaction was then evaluated (Scheme 1). Epoxides bearing linear alkyl chains of different lengths were well tolerated with excellent and good yields, from propylene oxide (R = $-CH_3$, 92%) to 1,2-epoxyhexane (R = $-(CH_2)_3CH_3$, 67%). However, moderate yields were observed in the case of longer alkyl chains (1,2-epoxytetradecane, R = $-(CH_2)_{11}CH_3$, 34%). Interestingly, a linear relationship with good fitting was found between conversion and number of C atoms in −R (Figure S29a), suggesting diffusion issues of the epoxide throughout the pores when increasing its size. This trend was extended for the rest of substrates in terms of molecular weight and length (Figure S29b-c), with the remarkable exception of styrene oxide and allyl glycidyl ether (19 and 53% yield, respectively). As all the substrates tested in this experiment were selected to enter inside pores (1.9 nm), we hypothesized that different hydrophobic and electrostatic interactions may occur between these two molecules and the MOF skeleton because of the presence of benzene rings and the oxygen of the ether group together with the double bond, respectively. These interactions were not remarkable for the rest of substrates, lacking benzene units, and showing one single O atom in the form of −OH (glycidol, 77% yield) or only one double bond (butadiene monoxide, 65% yield).

One of the main issues observed for (Zr)PCN-222(Co) was its limited stability after consecutive catalytic runs [12]. This fact was explained by the presence of TBAB as co-catalyst and the low stability of PCN-222 materials in basic media. To avoid this limitation, we evaluated the recyclability of (Hf)PCN-224(Co), exhibiting a higher chemical resistance and catalytic activity than the PCN-222 counterpart. Unlikely (Zr)PCN-222(Co), (Hf)PCN-224(Co) particles were not damaged after 7 consecutive runs, maintaining an

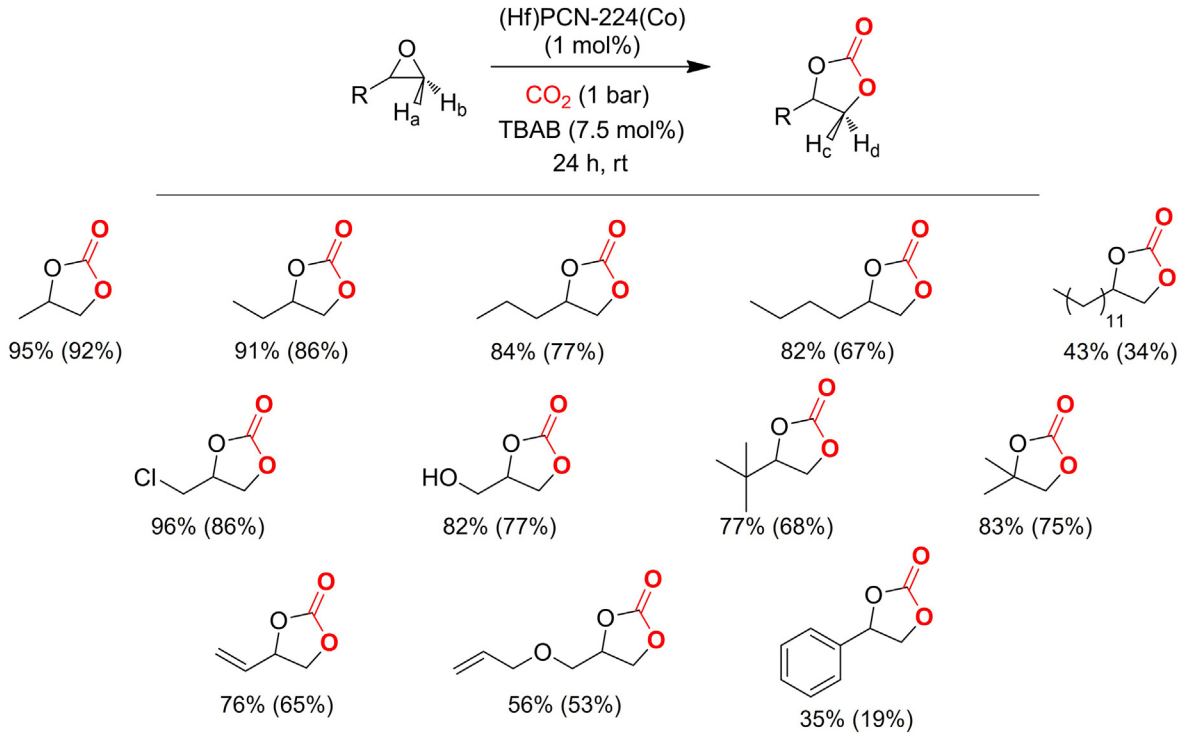

Scheme 1. Reaction scope.[a]
[a]Reaction conditions: 0.25 mmol epoxide, 1 mol% (Hf)PCN-224(Co), 7.5 mol% TBAB, 1 bar CO_2, 24 h, 24 °C. Conversions and yields (in parentheses) determined by ^{1}H-NMR spectroscopy calculating the ratio $H_{c/d}/(H_{a/b} + H_{c/d})$ and using 2,3,5,6-tetrachloronitrobenzene as internal standard, respectively.

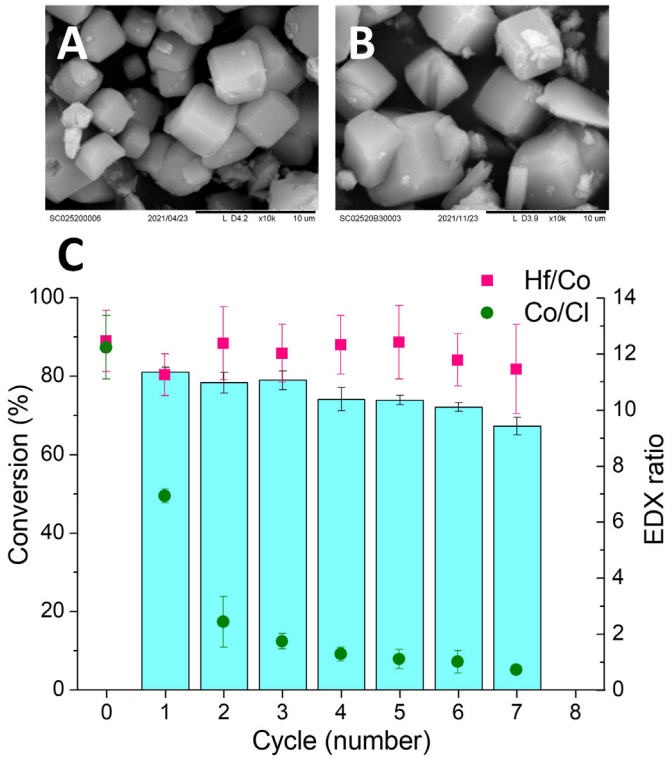

Fig. 3. Recyclability test. a) SEM images (x10000) of (Hf)PCN-224(Co): a) as-synthesized; b) after 7th cycle. c) Conversion (left y-axis) and EDX ratio (right y-axis) of Hf/Co (pink) and Co/Cl (green) found every catalytic cycle up to run 7. Conditions: 0.25 mmol epichlorohydrin, 1 mol% MOF, 7.5 mol% TBAB, 1 bar CO_2, 15 h, 24 °C. (For interpretation of the references to colour in this figure legend, the reader is referred to the Web version of this article).

excellent crystallinity (Figure S30) and well-defined size and shape (Fig. 3a and b). However, significant differences were interestingly found in terms of conversion between cycle 1 (81.0 ± 1.3%) and 4 (74 ± 3%), after which catalytic activity decreased a 9% compared to the original conversion. Further, performance decreased a 17% after run number 7 (Fig. 3c). Despite its excellent stability, we observed a progressive catalyst poisoning confirmed by X-EDS. Hf/Co elemental ratio was similar upon consecutive catalytic cycles (12.5 ± 1.1 after MOF synthesis and 11.5 ± 1.6 after 7 cycles), while Co/Cl ratio dramatically decreased for the same steps (12.2 ± 1.1 and 0.74 ± 0.11, respectively). The higher Cl content was related to the presence of remaining epichlorohydrin molecules attached to CUS, as previously demonstrated by ATR-FTIR (Figure S19). Similar C–H stretching bands from the epoxide, with their corresponding shifts, were observed after cycle 7 (Figure S31), suggesting this interaction.

We speculated that this effect was not mentioned nor observed before in CO_2 cycloadditions because: i) the typical epoxide used for catalysis optimization is propylene oxide, which had a negligible impact on CUS poisoning (Figure S20); ii) the presence of Cl favored the Hf/Co(MOF)-O(epoxide) interaction evidenced by ATR-FTIR (Figure S19) with significant C–H band shifts; and iii) this is the first work where a PCN-based catalyst was reused up to 7 consecutive catalytic runs (Fig. 3). Thus, the model epoxide demonstrated to be extremely challenging for recyclability tests. So, the regeneration thermal treatment (100 °C for 24 h) demonstrated to be effective to fully remove propylene oxide but not epichlorohydrin, not only because the higher interaction of the latter with the MOF, but also due to its higher boiling point. From these results, we evaluated this aspect through different regeneration tests performed at 150, 175 and 200 °C for 6 and 12 h (Figure S32). Interestingly, we recovered the initial catalytic activity in the cycle 8 after a simple thermal treatment at 175 °C for 6 h (82.4 ± 1.2% *vs.* 81.0 ± 1.3% in cycle 1). According to these results, we proposed that this thermal treatment should be applied after 3 consecutive catalytic runs to restore the initial performance of this MOF catalyst.

As far as we know, despite their catalytic potential and the evidences provided in this work, Hf porphyrin-MOFs have never been studied for CO_2 cycloadditions (Table S8). Although Zr porphyrin MOFs have demonstrated to work well, they usually requires from higher catalysts loadings [12], CO_2 pressures [18] and/or temperatures [58] than those described here. In addition, their recyclability has not been explored beyond the 4th catalytic run in all these cases, usually limiting the substrate scope to 1–5 epoxides. A similar epichlorohydrin conversion to that reported here was observed when a doubly Zn^{2+}/Co^{2+}-metalated (Zr)PCN-224 was pyrolyzed at 950 °C, and the resulting carbon-based material was used as catalyst at 50 °C for 20 h [59]. Other Hf-based MOFs lacking porphyrin linkers (*e.g.*, (Hf)VPI-100(Cu), (Hf)PCN-777 and (Hf)MOF-808) can achieve very high conversions for the same substrate (>96%) but only under more severe conditions (*e.g.* 80–90 °C and even, 10 bar CO_2) [60,61]. We suspect that the widespread attention paid to Zr porphyrin MOFs, although showing lower catalytic performance than Hf porphyrin MOFs, relies on their easier preparation under solvothermal conditions, while well-stablished synthetic protocols have not been reported yet for the hafnium counterparts.

4. Conclusions

In this work, we presented for the first time the assembly of metalated and non-metalated Hf based PCN-224 through a simple and efficient microwave-assisted synthesis with remarkable phase purity and good yields (>55%, STY>1100 kg m^{-3} day^{-1}). The influence of different acids as modulators was investigated, concluding that a strong acid such as trifluoromethanesulfonic acid was required to allow the coordination of the porphyrin linker and thus the MOF formation. Metalation was successfully performed in a 3-step, 1-pot fashion without further purification and tedious pre-synthetic linker modifications, enabling the presence of additional coordinatively unsaturated sites (CUS). These materials showed excellent textural properties and outstanding thermal (>340 °C) and chemical stabilities in different aqueous media (pH 1–11) and organic solvents, preserving their structural integrity even under harsh conditions (ultrasonic bath, and in the presence of HCl for 1 h and 60 °C).

As catalyst in CO_2 cycloaddition reactions with epoxides, (Hf)PCN-224(Co) displayed the best performance of all the porphyrin-based MOFs reported to date owing to: i) its exceptional stability; ii) the lower cluster coordination (6) compared to typical M^{4+}-carboxylate clusters (12 or 8 such as in UiO-66 or PCN-222, respectively), allowing for faster reagents diffusion and interaction with CUS; iii) the higher oxophilicity of the structural Hf^{4+} compared to Zr^{4+}; and iv) the synergy between the Brønsted and Lewis acid character of Hf^{4+} cluster and Co^{2+}, respectively. Besides, we evaluated 12 different epoxides, the largest scope tested to date with MOFs in this reaction, and the recyclability of the material up to unprecedented 8 cycles under mild conditions (room temperature, 1 bar CO_2, solvent-free reaction) with negligible loss of the initial catalytic activity upon a simple thermal regeneration treatment (175 °C, 6 h).

We expect that this work will provide a better understanding on the synthesis of Hf-based porphyrin MOFs, the importance of cluster stabilization prior linker coordination and the possibilities of microwave-assisted reactions in such MOF synthesis. Because of their potential, and the current limited scientific production in this

regard, this study paves the way for further producing and applying these MOFs not only for CO_2 cycloadditions with epoxides as acid catalysts, but also for other interesting catalytic applications, such as photo-/electro-chemical reductions to obtain green fuels, the development of optical sensors, drug delivery systems and photo(thermal) cancer therapy, among others.

Author contributions

Conceptualization, S.C. and P.H.; synthetic methodology and physicochemical characterization, S.C., G.O., G.C. and P.H.; TEM characterization, S.K., D.A.E., S.B; structural characterization, I.I. and D.M.; catalytic reactions, S.C., G.O., F.M., G.C.; resources, S.C, P.H., G.O., F.M., G.C.; writing, review and editing, all. All authors have read and agreed to the published version of the manuscript.

Funding sources

H2020-MSCA-COFUND GOT Energy Talent (ref. 754382), "Comunidad de Madrid" and European Regional Development Fund-FEDER 2014-2020-OE REACT-UE 1 for their financial support to VIRMOF-CM project associated to R&D projects in response to COVID-19, H2020-MSCA-ITN-2019 HeatNMof (ref. 860942), M-ERA-NET C-MOF-cell (grant PCI2020-111998 funded by MCIN/AEI /10.13039/501100011033 and European Union NextGenerationEU/ PRTR), Retos Investigación MOFSEIDON (grant PID2019-104228RB-I00 funded by MCIN/AEI/10.13039/501100011033).

Declaration of competing interest

The authors declare that they have no known competing financial interests or personal relationships that could have appeared to influence the work reported in this paper.

Data availability

Data will be made available on request.

Acknowledgment

S.C. acknowledges the European Union's Horizon 2020 research and innovation programme under the Marie Skłodowska-Curie (MSCA-COFUND) grant agreement No 754382 (GOT Energy Talent). S.C. and P.H. acknowledge "Comunidad de Madrid" and European Regional Development Fund-FEDER 2014-2020-OE REACT-UE 1 for their financial support to VIRMOF-CM project associated to R&D projects in response to COVID-19. The authors acknowledge H2020-MSCA-ITN-2019 HeatNMof (ref. 860942), the M-ERA-NET C-MOF-cell (grant PCI2020-111998 funded by MCIN/AEI /10.13039/ 501100011033 and European Union NextGenerationEU/PRTR) project, and Retos Investigación MOFSEIDON (grant PID2019-104228RB-I00 funded by MCIN/AEI/10.13039/501100011033) project. This work has been also supported by the Regional Government of Madrid (Project ACES2030-CM, S2018/EMT-4319) and the Universidad Rey Juan Carlos IMPULSO Project (grant MATER M – 3000). S.K acknowledges the Flemish Fund for Scientific Research (FWO Vlaanderen) through a PhD research grant (1181122 N).

Appendix A. Supplementary data

Supplementary data to this article can be found online at https://doi.org/10.1016/j.mtadv.2023.100390.

Abbreviations

MOF	metal-organic framework
PCN	porous coordination network
TCPP	5,10,15,20-(tetra-4-carboxyphenyl)porphyrin
ATR-FTIR	attenuated total reflection – Fourier transform infrared
X-EDS	energy-dispersive X-ray spectroscopy
ICP-OES	inductively coupled plasma - optical emission spectroscopy
TGA	thermogravimetric analysis
PXRD	powder X-ray diffraction
TBAB	tetrabutylammonium bromide
CUS	coordinatively unsaturated sites
FE-SEM	field emission – scanning electron microscopy
BET	Brauner-Emmet-Teller
UiO	Universitetet i Oslo
HAADF-STEM	high-angle annular dark-field scanning transmission electron microscopy

References

[1] F. Mehmood Mirza, A. Sinha, J. Rehman Khan, O.A. Kalugina, M. Wasif Zafar, Impact of energy efficiency on CO2 Emissions: empirical evidence from developing countries, Gondwana Res. 106 (2022) 64–77, https://doi.org/10.1016/j.gr.2021.11.017.
[2] W.F. Lamb, M. Grubb, F. Diluiso, J.C. Minx, Countries with sustained greenhouse gas emissions reductions: an analysis of trends and progress by sector, Clim. Pol. 22 (2022) 1–17, https://doi.org/10.1080/14693062.2021.1990831.
[3] G. Cohen, J.T. Jalles, P. Loungani, P. Pizzuto, Trends and cycles in CO2 emissions and incomes: cross-country evidence on decoupling, J. Macroecon. 71 (2022), 103397, https://doi.org/10.1016/j.jmacro.2022.103397.
[4] A. Kumar, P. Singh, P. Raizada, C.M. Hussain, Impact of COVID-19 on greenhouse gases emissions: a critical review, Sci. Total Environ. 806 (2022), 150349, https://doi.org/10.1016/j.scitotenv.2021.150349.
[5] I. Khan, A. Zakari, M. Ahmad, M. Irfan, F. Hou, Linking energy transitions, energy consumption, and environmental sustainability in OECD countries, Gondwana Res. 103 (2022) 445–457, https://doi.org/10.1016/j.gr.2021.10.026.
[6] A. Pommeret, F. Ricci, K. Schubert, Critical raw materials for the energy transition, Eur. Econ. Rev. 141 (2022), 103991, https://doi.org/10.1016/j.euroecorev.2021.103991.
[7] A. Valero, A. Valero, G. Calvo, A. Ortego, S. Ascaso, J.-L. Palacios, Global material requirements for the energy transition. An exergy flow analysis of decarbonisation pathways, Energy 159 (2018) 1175–1184, https://doi.org/10.1016/j.energy.2018.06.149.
[8] D. Yang, B.C. Gates, Catalysis by metal organic frameworks: perspective and suggestions for future research, ACS Catal. 9 (2019) 1779–1798, https://doi.org/10.1021/acscatal.8b04515.
[9] A. Bavykina, N. Kolobov, I.S. Khan, J.A. Bau, A. Ramirez, J. Gascon, Metal–organic frameworks in heterogeneous catalysis: recent progress, new trends, and future perspectives, Chem. Rev. 120 (2020) 8468–8535, https://doi.org/10.1021/acs.chemrev.9b00685.
[10] R. Freund, O. Zaremba, G. Arnauts, R. Ameloot, G. Skorupskii, M. Dincă, A. Bavykina, J. Gascon, A. Ejsmont, J. Goscianska, M. Kalmutzki, U. Lächelt, E. Ploetz, C.S. Diercks, S. Wuttke, The current status of MOF and COF applications, Angew. Chem. Int. Ed. 60 (2021) 23975–24001, https://doi.org/10.1002/anie.202106259.
[11] A.E. Baumann, D.A. Burns, B. Liu, V.S. Thoi, Metal-organic framework functionalization and design strategies for advanced electrochemical energy storage devices, Commun. Chem. 2 (2019) 86, https://doi.org/10.1038/s42004-019-0184-6.
[12] S. Carrasco, A. Sanz-Marco, B. Martín-Matute, Fast and robust synthesis of metalated PCN-222 and their catalytic performance in cycloaddition reactions with CO2, Organometallics 38 (2019) 3429–3435, https://doi.org/10.1021/acs.organomet.9b00273.
[13] M. Rimoldi, A.J. Howarth, M.R. DeStefano, L. Lin, S. Goswami, P. Li, J.T. Hupp, O.K. Farha, Catalytic zirconium/hafnium-based metal–organic frameworks, ACS Catal. 7 (2017) 997–1014, https://doi.org/10.1021/acscatal.6b02923.
[14] V.R. Bakuru, S.R. Churipard, S.P. Maradur, S.B. Kalidindi, Exploring the Brønsted acidity of UiO-66 (Zr, Ce, Hf) metal–organic frameworks for efficient solketal synthesis from glycerol acetalization, Dalton Trans. 48 (2019) 843–847, https://doi.org/10.1039/C8DT03512A.
[15] J. Jin, Porphyrin-based metal–organic framework catalysts for photoreduction of CO2: understanding the effect of node connectivity and linker metalation on activity, New J. Chem. 44 (2020) 15362–15368, https://doi.org/10.1039/D0NJ03507F.
[16] H. Su, M.S.G. Ahlquist, Nonbonded Zr4+ and Hf4+ models for simulations of condensed phase metal–organic frameworks, J. Phys. Chem. C 125 (2021)

6471–6478, https://doi.org/10.1021/acs.jpcc.1c00759.
[17] D. Feng, Z.-Y. Gu, J.-R. Li, H.-L. Jiang, Z. Wei, H.-C. Zhou, Zirconium-metalloporphyrin PCN-222: mesoporous metal–organic frameworks with ultrahigh stability as biomimetic catalysts, Angew. Chem., Int. Ed. 51 (2012) 10307–10310, https://doi.org/10.1002/anie.201204475.
[18] D. Feng, W.-C. Chung, Z. Wei, Z.-Y. Gu, H.-L. Jiang, Y.-P. Chen, D.J. Darensbourg, H.-C. Zhou, Construction of ultrastable porphyrin Zr metal–organic frameworks through linker elimination, J. Am. Chem. Soc. 135 (2013) 17105–17110, https://doi.org/10.1021/ja408084j.
[19] L. Wang, P. Jin, J. Huang, H. She, Q. Wang, Integration of copper(II)-Porphyrin zirconium metal–organic framework and titanium dioxide to construct Z-scheme system for highly improved photocatalytic CO2 reduction, ACS Sustain. Chem. Eng. 7 (2019) 15660–15670, https://doi.org/10.1021/acssuschemeng.9b03773.
[20] A. Bermejo-López, S. Carrasco, P.J. Tortajada, K.P.M. Kopf, A. Sanz-Marco, M.S. Hvid, N. Lock, B. Martín-Matute, Selective synthesis of imines by photo-oxidative amine cross-condensation catalyzed by PCN-222(Pd), ACS Sustain. Chem. Eng. 9 (2021) 14405–14415, https://doi.org/10.1021/acssuschemeng.1c04389.
[21] K. Sasan, Q. Lin, C. Mao, P. Feng, Incorporation of iron hydrogenase active sites into a highly stable metal–organic framework for photocatalytic hydrogen generation, Chem. Commun. 50 (2014) 10390–10393, https://doi.org/10.1039/C4CC03946G.
[22] K. Yu, D.-I. Won, W.I. Lee, W.-S. Ahn, Porphyrinic zirconium metal-organic frameworks: synthesis and applications for adsorption/catalysis, Kor. J. Chem. Eng. 38 (2021) 653–673, https://doi.org/10.1007/s11814-020-0730-z.
[23] M. Ding, X. Cai, H.-L. Jiang, Improving MOF stability: approaches and applications, Chem. Sci. 10 (2019) 10209–10230, https://doi.org/10.1039/C9SC03916C.
[24] T. He, X.-J. Kong, J.-R. Li, Chemically stable metal–organic frameworks: rational construction and application expansion, Acc. Chem. Res. 54 (2021) 3083–3094, https://doi.org/10.1021/acs.accounts.1c00280.
[25] S. Li, H.-M. Mei, S.-L. Yao, Z.-Y. Chen, Y.-L. Lu, L. Zhang, C.-Y. Su, Well-distributed Pt-nanoparticles within confined coordination interspaces of self-sensitized porphyrin metal–organic frameworks: synergistic effect boosting highly efficient photocatalytic hydrogen evolution reaction, Chem. Sci. 10 (2019) 10577–10585, https://doi.org/10.1039/C9SC01866B.
[26] J. Klinowski, F.A. Almeida Paz, P. Silva, J. Rocha, Microwave-assisted synthesis of metal–organic frameworks, Dalton Trans. 40 (2011) 321–330, https://doi.org/10.1039/C0DT00708K.
[27] P.P. Pescarmona, Cyclic carbonates synthesised from CO2: applications, challenges and recent research trends, Curr. Opin. in Green Sustain. Chem. 29 (2021), 100457, https://doi.org/10.1016/j.cogsc.2021.100457.
[28] A.J. Kamphuis, F. Picchioni, P.P. Pescarmona, CO2-fixation into cyclic and polymeric carbonates: principles and applications, Green Chem. 21 (2019) 406–448, https://doi.org/10.1039/C8GC03086C.
[29] S. Yuan, J.-S. Qin, C.T. Lollar, H.-C. Zhou, Stable metal–organic frameworks with group 4 metals: current status and trends, ACS Cent. Sci. 4 (2018) 440–450, https://doi.org/10.1021/acscentsci.8b00073.
[30] A. Mishra, T. Vats, J.H. Clark, Chapter 1 microwave radiations: theory and instrumentation, in: J. Clark (Ed.) Microwave-Assisted Polymerization, The Royal Society of Chemistry2016, pp. 1-18.
[31] Shaunak M. Shaikh, A. Chakraborty, J. Alatis, M. Cai, E. Danilov, A.J. Morris, Light harvesting and energy transfer in a porphyrin-based metal organic framework, Faraday Discuss 216 (2019) 174–190, https://doi.org/10.1039/C8FD00194D.
[32] R.S. Forgan, Modulated self-assembly of metal–organic frameworks, Chem. Sci. 11 (2020) 4546–4562, https://doi.org/10.1039/D0SC01356K.
[33] A.R. Byington, W.E. Bull, Trifluoromethanesulfonato complexes of nickel and cobalt, Inorg. Chim. Acta. 21 (1977) 239–244, https://doi.org/10.1016/S0020-1693(00)86268-4.
[34] A.U. Czaja, N. Trukhan, U. Müller, Industrial applications of metal–organic frameworks, Chem. Soc. Rev. 38 (2009) 1284–1293, https://doi.org/10.1039/B804680H.
[35] E. Alvarez, N. Guillou, C. Martineau, B. Bueken, B. Van de Voorde, C. Le Guillouzer, P. Fabry, F. Nouar, F. Taulelle, D. de Vos, J.-S. Chang, K.H. Cho, N. Ramsahye, T. Devic, M. Daturi, G. Maurin, C. Serre, The structure of the aluminum fumarate metal–organic framework A520, Angew. Chem. Int. Ed. 54 (2015) 3664–3668, https://doi.org/10.1002/anie.201410459.
[36] H.N. Sumedha, M.A. Alsaiari, M.S. Jalalah, M. Shashank, F.A. Alharthi, N. Ahmad, J.S. Algethami, V. Vishwanth, N. Ganganagappa, Rapid microwave synthesis of β-SnWO4 nanoparticles: an efficient anode material for lithium ion batteries, Crystals (2021) 11, https://doi.org/10.3390/cryst11040334.
[37] K.I. Hadjiivanov, D.A. Panayotov, M.Y. Mihaylov, E.Z. Ivanova, K.K. Chakarova, S.M. Andonova, N.L. Drenchev, Power of infrared and Raman spectroscopies to characterize metal-organic frameworks and investigate their interaction with guest molecules, Chem. Rev. 121 (2021) 1286–1424, https://doi.org/10.1021/acs.chemrev.0c00487.
[38] X. Wang, L. Andrews, Infrared spectrum and structure of the Hf(OH)4 molecule, Inorg. Chem. 44 (2005) 7189–7193, https://doi.org/10.1021/ic050614a.
[39] Y. Hou, X.-J. Hu, H.-Y. Tong, Y.-B. Huang, R. Cao, Unraveling the relationship of the pore structures between the metal-organic frameworks and their derived carbon materials, Inorg. Chem. Commun. 114 (2020), 107825, https://doi.org/10.1016/j.inoche.2020.107825.
[40] J.-J. Chen, L.-J. Wang, G.-J. Xu, X. Wang, R.-S. Zhao, Highly stable Zr(IV)-Based porphyrinic Metal–Organic frameworks as an adsorbent for the effective removal of gatifloxacin from aqueous solution, Molecules 23 (2018), https://doi.org/10.3390/molecules23040937.
[41] R.T. Cimino, P. Kowalczyk, P.I. Ravikovitch, A.V. Neimark, Determination of isosteric heat of adsorption by quenched solid density functional theory, Langmuir 33 (2017) 1769–1779, https://doi.org/10.1021/acs.langmuir.6b04119.
[42] D. Lv, R. Shi, Y. Chen, Y. Chen, H. Wu, X. Zhou, H. Xi, Z. Li, Q. Xia, Selective adsorptive separation of CO2/CH4 and CO2/N2 by a water resistant zirconium–porphyrin metal–organic framework, Ind. Eng. Chem. Res. 57 (2018) 12215–12224, https://doi.org/10.1021/acs.iecr.8b02596.
[43] O.K. Farha, K.L. Mulfort, A.M. Thorsness, J.T. Hupp, Separating solids: purification of metal-organic framework materials, J. Am. Chem. Soc. 130 (2008) 8598–8599, https://doi.org/10.1021/ja803097e.
[44] S. Leubner, R. Stäglich, J. Franke, J. Jacobsen, J. Gosch, R. Siegel, H. Reinsch, G. Maurin, J. Senker, P.G. Yot, N. Stock, Solvent impact on the properties of benchmark metal–organic frameworks: acetonitrile-based synthesis of CAU-10, Ce-UiO-66, and Al-MIL-53, chem, Eur. J. 26 (2020) 3877–3883, https://doi.org/10.1002/chem.201905376.
[45] U. Schubert, Clusters with a Zr6O8 core, Coord. Chem. Rev. 469 (2022), 214686, https://doi.org/10.1016/j.ccr.2022.214686.
[46] M.A. Luzuriaga, C.E. Benjamin, M.W. Gaertner, H. Lee, F.C. Herbert, S. Mallick, J.J. Gassensmith, ZIF-8 degrades in cell media, serum, and some—but not all—common laboratory buffers, Supramol. Chem. 31 (2019) 485–490, https://doi.org/10.1080/10610278.2019.1616089.
[47] Y. Chen, P. Li, J.A. Modica, R.J. Drout, O.K. Farha, Acid-resistant mesoporous metal–organic framework toward oral insulin delivery: protein encapsulation, protection, and release, J. Am. Chem. Soc. 140 (2018) 5678–5681, https://doi.org/10.1021/jacs.8b02089.
[48] F.D. Bobbink, F. Menoud, P.J. Dyson, Synthesis of methanol and diols from CO2 via cyclic carbonates under metal-free, ambient pressure, and solvent-free conditions, ACS Sustain. Chem. Eng. 6 (2018) 12119–12123, https://doi.org/10.1021/acssuschemeng.8b02453.
[49] G. Trott, P.K. Saini, C.K. Williams, Catalysts for CO2/epoxide ring-opening copolymerization, Philos. Trans. Royal Soc. A 374 (2016), 20150085, https://doi.org/10.1098/rsta.2015.0085.
[50] X. Liang, F. Tan, Y. Zhu, Recent developments in ring-opening copolymerization of epoxides with CO2 and cyclic anhydrides for biomedical applications, Front. Chem. 9 (2021), 647245, https://doi.org/10.3389/fchem.2021.647245.
[51] E. Liu, J. Zhu, W. Yang, F. Liu, C. Huang, S. Yin, PCN-222(Co) metal–organic framework nanorods coated with 2D metal–organic layers for the catalytic fixation of CO2 to cyclic carbonates, ACS Appl. Nano Mater. 3 (2020) 3578–3584, https://doi.org/10.1021/acsanm.0c00305.
[52] H. Zhang, J. Wei, J. Dong, G. Liu, L. Shi, P. An, G. Zhao, J. Kong, X. Wang, X. Meng, J. Zhang, J. Ye, Efficient visible-light-driven carbon dioxide reduction by a single-atom implanted metal–organic framework, Angew. Chem. Int. Ed. 55 (2016) 14310–14314, https://doi.org/10.1002/anie.201608597.
[53] L. Feng, K.-Y. Wang, E. Joseph, H.-C. Zhou, Catalytic porphyrin framework compounds, Trends Chem 2 (2020) 555–568, https://doi.org/10.1016/j.trechm.2020.01.003.
[54] D. Bai, S. Duan, L. Hai, H. Jing, Carbon dioxide fixation by cycloaddition with epoxides, catalyzed by biomimetic metalloporphyrins, ChemCatChem 4 (2012) 1752–1758, https://doi.org/10.1002/cctc.201200204.
[55] B.N. Cabral, J.L.S. Milani, A.M. Meireles, D.C.d.S. Martins, S.L.d.S. Ribeiro, J.S. Rebouças, C.L. Donnici, R.P. das Chagas, Mn(iii)–porphyrin catalysts for the cycloaddition of CO2 with epoxides at atmospheric pressure: effects of Lewis acidity and ligand structure, New J. Chem. 45 (2021) 1934–1943, https://doi.org/10.1039/D0NJ05280A.
[56] X. Jiang, F. Gou, F. Chen, H. Jing, Cycloaddition of epoxides and CO2 catalyzed by bisimidazole-functionalized porphyrin cobalt(iii) complexes, Green Chem. 18 (2016) 3567–3576, https://doi.org/10.1039/C6GC00370B.
[57] Y. Ren, J. Chen, C. Qi, H. Jiang, A new type of Lewis acid–base bifunctional M(salphen) (M=Zn, Cu and Ni) catalysts for CO2 fixation, ChemCatChem 7 (2015) 1535–1538, https://doi.org/10.1002/cctc.201500113.
[58] L. Zhang, S. Yuan, W. Fan, J. Pang, F. Li, B. Guo, P. Zhang, D. Sun, H.-C. Zhou, Cooperative sieving and functionalization of Zr metal–organic frameworks through insertion and post-modification of auxiliary linkers, ACS Appl. Mater. Interfaces 11 (2019) 22390–22397, https://doi.org/10.1021/acsami.9b05091.
[59] J. Ji, H. Liu, Z. Chen, Y. Fu, W. Yang, S.-F. Yin, Modulating the acidic and basic site concentration of metal-organic framework derivatives to promote the carbon dioxide epoxidation reaction, Chem. Eur J. 27 (2021) 11102–11109, https://doi.org/10.1002/chem.202100430.
[60] J. Zhu, J. Liu, Y. Machain, B. Bonnett, S. Lin, M. Cai, M.C. Kessinger, P.M. Usov, W. Xu, S.D. Senanayake, D. Troya, A.R. Esker, A.J. Morris, Insights into CO2 adsorption and chemical fixation properties of VPI-100 metal–organic frameworks, J. Mater. Chem. 6 (2018) 22195–22203, https://doi.org/10.1039/C8TA06383D.
[61] L. Jin, Q. Qin, L. Dong, S. Liu, S. Xie, J. Lu, A. Xu, J. Liu, H. Liu, Y. Yao, X. Hou, M. Fan, Study of the cycloaddition of CO2 with styrene oxide over six-connected spn topology MOFs (Zr, Hf) at room temperature, Chem. Eur J. 27 (2021) 14947–14963, https://doi.org/10.1002/chem.202102408.